Journal of Thermal Analysis and Calorimetry, 83 (2006) 2, 507–518

PHYSICAL PROPERTIES OF NON-STOICHIOMETRIC OXIDES
Superconducting oxides

A. Caneiro[*], *F. Prado and A. Serquis*

Centro Atómico Bariloche, CNEA, (8400) S. C. de Bariloche, Pcia. de Río Negro, Argentina

An important example of oxide materials exhibiting oxygen non-stoichiometry are the high temperature superconductors (HTSC). In this family of materials the variation of the oxygen content modifies the defect structure and the carrier concentration, causing phase transitions and structural distortions with the consequent change in their physical properties. In some systems, a continuous variation of the physical properties as a function of the oxygen content is observed, while in others, small changes of the oxygen content strongly modify the superconducting behavior of these materials. In this paper, we review an analysis of the influence of the oxygen content on the physical properties of three HTSC materials: the electron doped Nd–Ce–Cu–O superconductor, the R–Ba–Cu–O (*R*=Nd, Gd, Pr) 123 compounds and the (Hg, Re)-1201 material.

Keywords: *non-stoichiometric oxides, superconductors (HTSC)*

Introduction

It is well-known the influence of the oxygen content on the superconducting properties of the HTSC materials. A large number of papers have been published analyzing this effect. However, for several systems, significant disagreements can be found between different works. This may be due to poorly characterized samples and not well-known oxygen content values.

The effect of the oxygen content on the physical properties is qualitatively reported in most of the papers for samples annealed under different conditions without an accurate knowledge of their oxygen content. For some systems, this effect is dramatic, leading to superconducting or non-superconducting samples after very small changes on their oxygen stoichiometry.

One of this examples is the electron doped material of general formula $Ln_{2-x}(Ce,Th)_xCuO_y$ (*Ln*=Nd, Sm, Pr and Eu) with the Nd_2CuO_4-type crystalline structure (T'-phase). The main features of this system are the square-planar coordination of the Cu ions by oxygen atoms and the extreme sensitivity of its superconducting response to small variations in the dopant content (Ce, Th) '*x*' or oxygen content '*y*'. For instance, as-made samples are not superconducting and the superconducting ones are achieved by annealing them at $850<T_q$ (°C)<1150 under oxygen partial pressure $p(O_2)$ between 10^{-6} and 10^{-3} atm. and subsequent quenching [1, 2]. The role of this treatment ('reduction step') in the appearance of superconductivity has been extensively discussed. It is evident that oxygen atoms are removed during the reduction step. The question concerning which are the oxygen sites in the structure involved in this process seems now to be clear. It is accepted that interstitial oxygen atoms located at the apical sites of the T'-phase structure are removed during this treatment. However, the amount of oxygen removed is very small, with values ranging between 0.01 and 0.05 per unit formula [3–13]. The open question now is that this amount is too small to explain the induction of superconductivity as only due to a variation of the carrier concentration.

The second example is one of the most studied HTSC materials: the 123 compounds. The 123 phase can be obtained for $YBa_2Cu_3O_y$ and also replacing *Y* by most of the rare earth elements, exceptions being Ce, Pm, Tb. The $RBa_2Cu_3O_y$ (*R*=La, Nd, Sm, Eu, Gd, Ho, Y, Er, Tm, Yb) compounds display a wide range of oxygen non-stoichiometry with '*y*' values ranging between 6 and 7. Such wide range of '*y*' values accepted by 123 phase strongly modify the critical temperature (T_c) and promote an order/disorder orthorhombic/tetragonal (*O*/*T*) phase transition. Despite the large number of papers concerning the physical properties of these R123 (*R*=La, Nd, Sm, Eu, Gd, Ho, Y, Er, Tm, Yb) compounds, only few studies have been reported in the literature on their high temperature thermodynamic properties and the *O*/*T* transition [14–20].

Another example of disagreements between different works concerning the influence of the oxygen content on the superconducting properties is the $HgBa_2CuO_y$ compound (Hg-1201) [21–25]. These differences are mainly due to the difficulties to obtain single phase materials and to determine accurately the

* Author for correspondence: caneiro@cab.cnea.gov.ar

1388–6150/$20.00

Akadémiai Kiadó, Budapest, Hungary
Springer, Dordrecht, The Netherlands

oxygen content of the samples. The high vapor pressure of Hg and the high reactivity of Ba compounds with water vapor and carbon dioxide make the synthesis of single phase materials difficult. Besides, the absolute oxygen content of the samples can not be determined by thermogravimetry due to the high vapor pressure of Hg. As an alternative, the oxygen content can be obtained by either iodometric titration or neutron powder diffraction data refinements. However, the oxygen content values obtained with both techniques show significant differences [21–25].

It is known that the incorporation of transition metals (Re, W, V, etc.) in the $HgBa_2CuO_y$ compound improves their chemical stability [26]. Nevertheless, there are not detailed studies on the role of transition elements on the superconducting response of the Hg-1201 compound.

The aim of this paper is to review our results for three selected HTCS superconductors to show the useful and essential information obtainable by a thermal analysis (TA) technique such as thermogravimetry (TG) under controlled atmospheres. TG is currently used to characterize HTSC materials and precursors used in their synthesis. Thus, TG has been widely used to study precursors materials used in the synthesis of HTSC [27, 28], the thermal and phase stabilities of HTSC materials [29, 30], the thermodynamic properties and defect structure [31, 32], surface properties of 123 materials [33], etc. Particularly, we want to emphasize the convenience of using thermogravimetry under controlled atmosphere [34] for the characterization of these materials. The determination by thermogravimetry of the equilibrium oxygen partial pressure $p(O_2)$ as a function of both temperature and oxygen content provide valuable information on the high temperature range of stability and defect structure of non-stoichiometric oxides. These high temperature thermodynamic data also allow the preparation of samples with accurate control of the oxygen content and therefore the study of their physical properties.

For the $Nd_{1.85}Ce_{0.15}CuO_y$ compound, we show through both $p(O_2)$ and resistivity measurements at high temperatures the existence of two types of defects: oxygen vacancies and interstitial oxygen atoms. The superconducting response of samples with accurate control of the oxygen content is strongly correlated with the presence of such defects.

For the $RBa_2Cu_3O_y$ (*R*=Y, Gd, Nd)123 compounds, we present equilibrium $p(O_2)$ data at high temperatures. The effect of the ionic size of the *R* atom on the oxygen non-stoichiometry and phase stability of R123 compounds at high temperatures is discussed.

Finally, for the Re doped Hg-1201 materials ($Hg_{1-x}Re_xBa_2CuO_y$), we demonstrate by means of $p(O_2)$ measurements the effect of the Re content on the improvement of the thermal stability of the 1201 phase. We will also discuss the role of the oxygen excess on the critical temperature.

Experimental

Materials

Samples of $Nd_{1.85}Ce_{0.15}Cu_{1.01}O_y$ with a Cu excess of 1% and accurate control of oxygen content were prepared by the liquid mix method (LMM), using Nd_2O_3, metallic Ce and Cu as raw materials. A small Cu excess in the samples is needed to avoid the presence of Cu vacancies in the Cu–O planes which affect the superconducting response of this material [35]. The LMM method was chosen because it yields samples with a more homogeneous Ce distribution than the usual solid state reaction one [36].

Ceramic samples of Gd123 and Nd123 were also prepared following the liquid-mix method with R_2O_3 (*R*=Gd, Nd), $BaCuO_3$ and metallic Cu as raw materials. The Y123 was manufactured by Seattle Specialty Ceramics (SSC, Inc.) with particle size ranging between 2 and 6 μm.

Samples of $Hg_{1-x}Re_xBa_2CuO_y$ were prepared following the method proposed by Alyoshin *et al.* [37]. High purity HgO, ReO_3, CuO and BaO were the raw materials for these samples. The synthesis of the 1201 phase was performed in sealed quartz capsules under controlled $p(O_2)$.

Methods

Equilibrium $p(O_2)$ data as a function of temperature and oxygen content were performed using a high sensitive thermogravimetric equipment [34] consisting of a symmetrical thermobalance based on a Cahn 1000 electrobalance coupled to an electrochemical gas blending system. The electrochemical system (zirconia pump and oxygen sensor) provides a controlled $Ar–O_2$ or $CO–CO_2$ atmospheres for the thermobalance with $p(O_2)$ values ranging between $1\cdot10^{-14}$ and 1 atm. Figure 1a depicts a block diagram of the thermobalance and the electrochemical system. In Fig. 1b, the design of the hangdown tubes of the thermobalance is shown.

The error in $p(O_2)$ for the $Ar–O_2$ mixtures can be estimated as approximately 2% (including systematic ones). The thermobalance allows the detection of changes in '*y*' within 0.0005 for a sample of about 1 g. The equilibrium criterion used in this work, verified over of the 24 h periods, was constant sample mass with time within 10 μg.

The absolute oxygen content of the $Nd_{1.85}Ce_{0.15}Cu_{1.01}O_y$ and $RBa_2Cu_3O_y$ (*R*=Y, Gd, Nd)

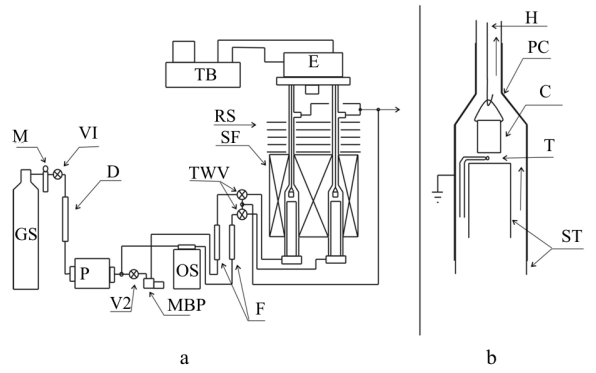

Fig. 1 a – Block diagram of the experimental setup. G. S. – gas source; M – manometer; V1,V2 – needle valves; D – drying column; P – electrochemical pump; OS – oxygen sensor; F – flowmeter; MBP – metal bellow pump; TWV – three-way valve; SF – symmetrical furnace; RS – radiation shields; TB – thermostatic bath; E – electrobalance. b – ST, silica tubes; T – Pt–Pt10% Rh thermocouple; C – alumina crucible; H – hangdown wire; PC – platinum coating

samples were determined after performing the thermogravimetric measurements by in situ reduction in dry H_2 at 1150°C assuming Nd_2O_3, Ce_2O_3, R_2O_3 and metallic Cu as reduction products.

The absolute oxygen content of the $Hg_{1-x}Re_xBa_2CuO_y$ samples was determined by thermogravimetry and Rietveld refinements of the neutron powder diffraction data.

Samples with controlled oxygen content were prepared by annealing them at different T and $p(O_2)$ values during periods ranging between 12 and 48 h and later quenching at liquid nitrogen temperature.

High temperature electrical resistivity measurements were carried out simultaneously with the thermogravimetric ones by a standard four-probe ac technique with a lock-in amplifier on a dense sample placed 2 mm below the crucible of the balance.

Powder X-ray diffraction (XRD) data were recorded on a Philips PW-1700 diffractometer using CuK_α radiation and a graphite monochromator. The collection time by steps of 0.02^o was 10 s. X-ray data of the samples were refined by the Rietveld method with the DBWS-9411 program [38]. High temperature X-ray powder diffraction data were obtained making use of an Anton Paar HTK-10 camera coupled to the diffractometer. The $p(O_2)$ within the camera was controlled by means of flowing N_2–O_2 mixtures supplied by an electrochemical system similar to that used in the thermobalance.

Differential thermal analysis (DTA) curves were recorded with a Netzsch STA 409 analyzer while heating the samples from room temperature up to 1200°C at a heating rate of 10°C min^{-1} under pure O_2.

The presence of superconductivity was detected through dc magnetization (M) measurements with a Quantum Design SQUID magnetometer.

Results and discussion

$Nd_{1.85}Ce_{0.15}Cu_{1.01}O_y$ material

In Fig. 2, the equilibrium $p(O_2)$ measurements at 900°C are plotted as a function of oxygen content 'y' for the $Nd_{1.85}Ce_{0.15}Cu_{1.01}O_y$ sample. The 'reduction step' is usually performed at 900°C, while the $p(O_2)$ range in Fig. 2 covers the $p(O_2)$ values normally used for this heat treatment.

The shape of this isotherm is similar to those reported in [13, 31]. The starting point A was obtained after an annealing treatment at 900°C for 48 h under pure O_2. Next, the $p(O_2)$ was successively lowered to point B. Between points A and B, the time required to approach equilibrium after a change of $p(O_2)$ was fairly long, typically 24 to 48 h.

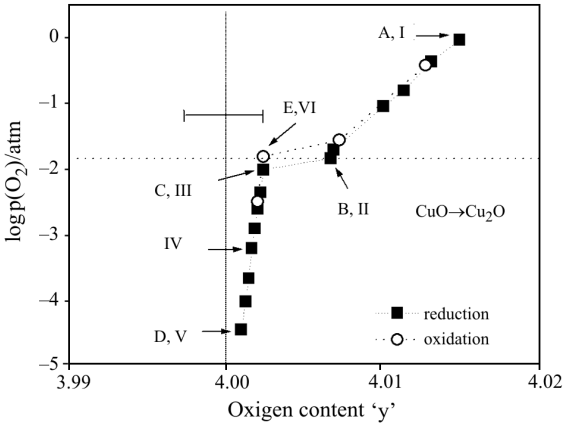

Fig. 2 Log$p(O_2)$ *vs*. oxygen content curve at 900°C for the $Nd_{1.85}Ce_{0.15}Cu_{1.01}O_y$ sample. The bar indicates the error in the absolute oxygen content 'y'

From point B, and after a small decrement of $p(O_2)$, a continuous and slow mass of the sample is observed reaching finally after 48 h the composition corresponding to point C. The average value of $p(O_2)$ between those corresponding to points B and C agrees with that of the Cu_2O–CuO equilibrium. Therefore, we associate the discontinuity of the sample mass as a function of $p(O_2)$ to the reduction of CuO traces into Cu_2O contained in the sample. From the mass loss between points B and C, the amount of free CuO present in the sample can be estimated as 0.16% *w/o* (corresponding to an extra Cu atomic concentration of 0.8%).

By lowering gradually $p(O_2)$ from point C, equilibrium points up to point D were obtained. The time necessary to reach equilibrium for the points between

C and D was 10 times lower than that of points between A and B. By increasing $p(O_2)$ from point D the data points up to point E were obtained. A hysteretic effect is detected around the $p(O_2)$ value corresponding to the CuO–Cu_2O equilibrium.

For $p(O_2)$ values higher than that of the CuO–Cu_2O equilibrium, oxygen excess should be present in the sample. For $p(O_2)$ values lower than the CuO–Cu_2O equilibrium one, the thermodynamic data indicate oxygen deficiency.

The shape of this isotherm gives useful qualitative information on the nature of the oxygen defects present in the sample [36]. For $p(O_2)$ values higher than the CuO–Cu_2O equilibrium one, the oxygen excess should be related to the existence of interstitial oxygen atoms located in the apical site of the T'-phase structure. For $p(O_2)$ lower than the CuO–Cu_2O equilibrium value, oxygen vacancies should be present in the sample. Thus, the $p(O_2)$ isotherm shows two well differentiated parts: A–B and C–D–E (Fig. 2). Each of them is characterized by a different type of oxygen defects.

The presence of these defects in the $Nd_{1.85}Ce_{0.15}Cu_{1.01}O_y$ sample can be confirmed by complementary measurements such as high temperature resistivity ρ *vs*. $p(O_2)$ data at constant temperature.

Usually, the resistivity measurements are performed as a function of temperature in samples with a starting oxygen content value. However, it is very difficult to keep constant the oxygen content '*y*' in measurements where the temperature is varied. Thus, it is hard to establish from this information if the variations in ρ are due to a change in the carrier concentration or in the scattering centers.

Considering this complication, we performed ρ *vs*. $p(O_2)$ measurements at constant temperature inside the thermobalance on a parallelepiped sample placed a few millimeters below the crucible. Thus, both samples, one placed in the crucible of the thermobalance and the other one for resistivity are at identical temperature and surrounding by the same atmosphere. Therefore, it is possible to correlate both the resistivity and the mass variations of the sample with $p(O_2)$.

Figure 3 shows the ρ *vs*. log$p(O_2)$/atm data for the $Nd_{1.85}Ce_{0.15}Cu_{1.01}O_y$ sample. It can be observed that the resistivity decreases with the log$p(O_2)$ from zero to –1.84 approximately and then remains almost constant up to log($p(O_2)$/atm)≈–4.00. The decrease of ρ agrees with the presence of oxygen excess as detected by thermogravimetry. Therefore, this dependence should indicate the nature of the oxygen defects present in the sample for this range of $p(O_2)$.

A simple method to analyze the behavior of the conductivity as a function of $p(O_2)$ is to use the formalism of the defect chemistry involving the mass action law. This law can also be applied in order to find

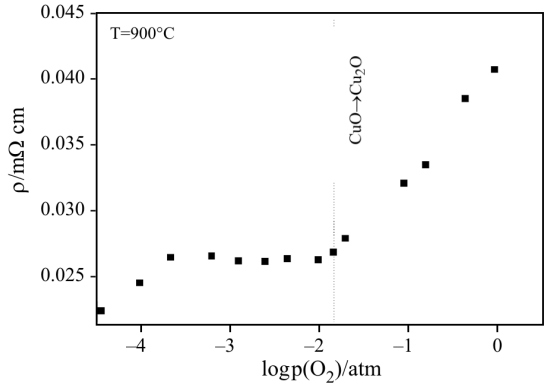

Fig. 3 ρ *vs*. log$p(O_2)$ data for the $Nd_{1.85}Ce_{0.15}Cu_{1.01}O_y$ sample

a relationship between the deviation of the oxygen stoichiometry and log$p(O_2)$. However, the variation of the oxygen content measured in this sample is too small and comparable to its absolute error. Therefore, in the present case it is more convenient to apply the mass action law for conductivity data instead of oxygen content deviations.

According to this formalism, the formation of simple point defects within the region where oxygen vacancies are the predominant defects can be written using the Kröger–Vink notation [39]:

$$O_o = V_o^{\bullet\bullet} + 1/2O_2(g) + 2e' \quad (1)$$

and

$$1/2O_2(g) = O_i'' + 2h^{\bullet} \quad (2)$$

for the region where interstitial oxygen atoms are the predominant defect.

From Eqs (1) and (2) the electrical conductivity as a function of $p(O_2)$ is given by:

$$\sigma \propto n \propto [\log p(O_2)^{-1/6}]$$
$$p << n \text{ for oxygen vacancies} \quad (3)$$

$$\sigma \propto p \propto [\log p(O_2)^{1/6}]$$
$$n << p \text{ for interstitial oxygen} \quad (4)$$

where $n = [e']$ *and* $p = [h^{\bullet}]$.

However, in the $Nd_{1-x}Ce_xCu_{1+\delta}O_y$ material, the conductivity is given by the Ce doping and the oxygen defects. Therefore, the electroneutrality equation is:

$$[V_o^{\bullet\bullet}] + [Ce_{Nd}^{\bullet}] = [e'] + 2[O_i''] \quad (5)$$

For the $p(O_2)$ region where the predominant defects are interstitial oxygen atoms, the oxidation reaction is given by:

$$1/2O_2 + 2e' \leftrightarrow O_i'' \quad (6)$$

For $[Ce_{Nd}^{\bullet}]=0.15$ and $[V_o^{\bullet\bullet}]=0$, from Eqs (5) and (6), a relationship between $p(O_2)$ and the carrier concentration is obtained:

$$K = \frac{[p(O_2)]^{1/2} n^2}{1/2(0.15 - n)} \quad (7)$$

In Fig. 4, we plot logσ *vs.* log[$p(O_2)$]. For $-4<\log(p(O_2)/\text{atm})<-1.84$, the conductivity remains almost constant indicating that the contribution to the total conductivity is mainly due to the Ce doping. For $\log(p(O_2)/\text{atm})>-1.84$ the conductivity decreases 10% for an increment of the oxygen content of about 0.25% (4.00 to 4.01).

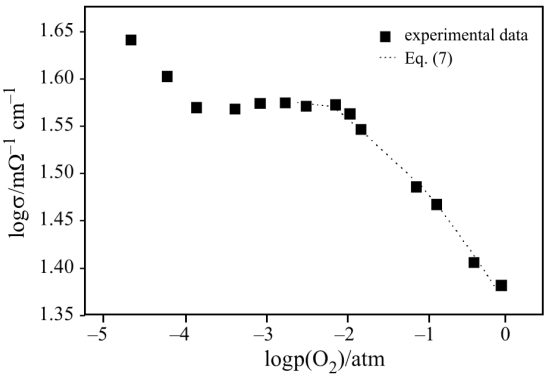

Fig. 4 Logσ *vs*. log$p(O_2)$ at 900°C for the $Nd_{1.85}Ce_{0.15}Cu_{1.01}O_y$ sample

In Fig. 4, the relation between σ and $p(O_2)$ determined by Eq. (7) is also plotted, assuming that σ is proportional to the carrier concentration. A good agreement between the experimental data and this equation was found. The proportionality constant between σ and *n* was determined from the conductivity data within the region $-4.00<\log(p(O_2)/\text{atm})<-1.84$ where σ is constant and mainly due to Ce doping.

Considering the 4+ oxidation state of Ce in the T'-phase structure, a concentration of [Ce]=0.15 gives a carrier concentration of $1.6\cdot10^{21} e^- cm^{-3}$. For an increment in the oxygen content of 0.008 per unit formula, the variation in the carrier concentration is about $2\cdot10^{20} e^- cm^{-3}$, which corresponds to a 12% of the carrier concentration given by the Ce doping. This rough estimation agrees with our observed variation in the conductivity. This result also indicates that the variations in the resistivity data are due to a bulk effect.

Figure 5 shows the Meissner fraction (FC measurements) *vs*. *T* for samples of $Nd_{1.85}Ce_{0.15}Cu_{1.01}O_y$ prepared with accurate control of the oxygen content. The samples were obtained by annealing at 900°C for 24 h under $p(O_2)$ values corresponding to points I to VI indicated in Fig. 2 and subsequent quenching to liquid nitrogen.

It can be observed the lack of superconductivity for samples quenched from $p(O_2)$ values where CuO is stable over Cu_2O (points I and II). The superconductivity suddenly appears for samples quenched from $p(O_2)$ values where Cu_2O is stable over CuO. This experimental evidence has been already reported by Kim *et al.* [12] and Prado *et al.* [40] and more recently confirmed by Raman spectroscopy [41].

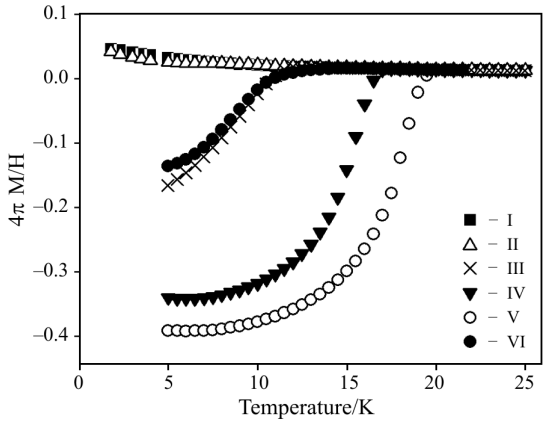

Fig. 5 Meissner fraction as a function of temperature for samples prepared after quenching from $p(O_2)$ and oxygen content of points I, II, III, IV, V and VI indicated in Fig. 2

In Table 1, the T_{co} (onset critical temperature) values measured for the $Nd_{1.85}Ce_{0.15}Cu_{1.01}O_y$ sample as a function of the oxygen content '*y*' are listed. The '*y*' values were corrected taking into account the presence of CuO traces [40].

Table 1 Oxygen content and T_{co} for $Nd_{1.85}Ce_{0.15}Cu_{1.01}O_y$ samples quenched from $p(O_2)$ indicated in Fig. 2 [32]

Sample	Oxygen content/*y*	T_{co}/K
I	4.00789	–
II	3.99967	–
III	3.99953	12
IV	3.99897	17
V	3.99841	20
VI	3.99958	14

It is interesting to compare the superconducting behavior of samples II, III and VI. These samples were quenched at almost the same $p(O_2)$ and exhibit very close oxygen content values. However, sample II does not show any superconducting response while samples III and VI show a diamagnetic signal with a depressed $T_{co}\approx12$ K.

The relevant question is if the oxygen loss between sample II and III is due to the reduction of the T'-phase or to the reduction of CuO into Cu_2O. Both possibilities lead to different interpretations on the role of the reduction step.

Assuming that the oxygen content loss between sample II and III corresponds to the T'-phase, the difference in the overall oxygen content between both samples is 0.0043 (Fig. 2). This value corresponds to an average distance among interstitial oxygen atoms

of ~25 Å. This distance is in the range of the in-plane coherence length (ξ) and could affect the superconducting response. In this case, the oxygen chemical potential which separates interstitial oxygen atoms and oxygen vacancies should accidentally coincide with that of the Cu_2O/CuO equilibrium. However, if we consider that the jump in Δy around $p(O_2)$ (Cu_2O/CuO) is due to the reduction of CuO into Cu_2O, the variation on the oxygen content assigned to the T'-phase between these two samples is as low as 0.0001; this value is appreciably lower than the difference in the overall oxygen content between both samples. In this case the average distance between interstitial oxygen atoms is ~85 Å. This value is higher than ξ, and therefore for this case the lack of superconductivity in sample II is hard to attribute solely to the presence of interstitial oxygen atoms.

The existence of chemical hysteresis for $p(O_2)$ around the Cu_2O–CuO equilibrium value suggests another interpretation for the role of the reduction step.

We think that the analysis of the hysteresis effect observed in the log$p(O_2)$ *vs.* '*y*' data around the Cu_2O–CuO equilibrium oxygen partial pressure is the key to understand this puzzling behavior of the superconducting response of $Nd_{1.85}Ce_{0.15}Cu_{1.01}O_y$ as a function of the annealing $p(O_2)$.

The chemical hysteresis causes multivaluated $p(O_2)$ for a given oxygen content. Thus, the Gibbs rule that anticipate a unique $p(O_2)$ value for the two-phase region cannot be applied. The hysteretic behavior in $p(O_2)$ has been extensively discussed in the literature, particularly for rare-earth oxides [42, 43], and is associated to the existence of two solid phases with close structural relationship between them. This condition is required to create coherent interfaces or semi-coherent interfaces with low interfacial free energy and a non-negligible elastic strain energy (ΔGs). The contribution of ΔGs must be added to that of the phase (T'-phase in our case) in order to describe the total Gibbs energy of the system (G) and therefore the oxygen chemical potential. Hence, the existence of hysteresis in the equilibrium $p(O_2)$ measurements around a phase transformation strongly suggests the presence of intergrowth between both phases. In the present case, this effect could be due to intergrowth between the T'-phase and CuO. This hypothesis is based on the similar coordination of Cu ions in both structures.

The Cu_2O structure is cubic. In this material the oxygen atoms are located in a bcc arrangement where each oxygen atom is surrounded by four Cu ions in a tetrahedral coordination. On the other hand, the CuO structure can be described in the C_c monoclinic space group with lattice parameters a=4.6927 Å, b=3.4283 Å, c=5.1370 Å and β=99.54° at room temperature. In this structure, the Cu ions are coordinated by four coplanar oxygen atoms forming an almost rectangular parallelogram, while the oxygen coordination polyhedron has four Cu ions at the corners of a distorted tetrahedron. The CuO_4 units, by sharing opposite edges, form two ribbons of parallelograms running in the [110] and [$\bar{1}$10] directions. The distances between the Cu ions and the four oxygen in the CuO_4 unit are: 2.041, 1.956, 1.958 and 1.886 Å [44] and in the case of the T'-phase the Cu–O distance is approximately 1.972 Å. Thus, it is possible that the CuO_4 units of the CuO phase intergrowth with CuO_2 planes of the T'-phase. As a consequence, microstrains should be generated around the T'/CuO interface. These microstrains should increase the oxygen solubility in the T'-phase giving rise to the presence of interstitial oxygen defects when the $p(O_2)$ is higher than that of equilibrium Cu_2O–CuO. When Cu_2O is in equilibrium with the T'-phase, intergrowth between these two phases is difficult due to the structural differences between them. The Cu ions are planar coordinated with four oxygen atoms in the T'-phase structure while the Cu ions are tetrahedrally coordinated with the oxygen atoms in the Cu_2O phase.

Therefore, for $p(O_2)$ values where the T'-phase is in equilibrium with Cu_2O, the T'-phase is free of microstrains and superconductivity is induced in samples quenched from these $p(O_2)$ values. In the present picture, the presence of interstitial oxygen atoms is a consequence of the existence of microstrains caused by the intergrowth between the CuO and the T'-phase. The T'-phase is a close-packet structure and therefore, there is not enough available space for the location of interstitials atoms such as oxygen excess. However, microstrains caused by the intergrowth between the CuO and the T'-phase could permit the location of a small concentration of oxygen excess in the T'-structure as it is observed by our thermogravimetry measurements for $p(O_2)$ higher than that of the CuO/Cu_2O equilibrium. These results suggest that CuO might intergrowth with the CuO_2 planes of the T' structure leading to a subtle internal strain that quenches the superconducting state.

$RBa_2Cu_3O_y$ (R=Y, Gd, Nd) material

In Fig. 6 are displayed the isobars determined under 1 atm of pure O_2 for Y123 (solid circles), Gd123 (open circles) and Nd123 (square solid lines). The symbols correspond to equilibrium values after a step change in temperature, while the solid lines were determined at a heating constant rate of 1°C min^{-1}. The agreement between both procedures show that the release of oxygen in R123 compound is a rapid process even at moderate temperatures. These curves contain very useful information. On one hand, it can be ob-

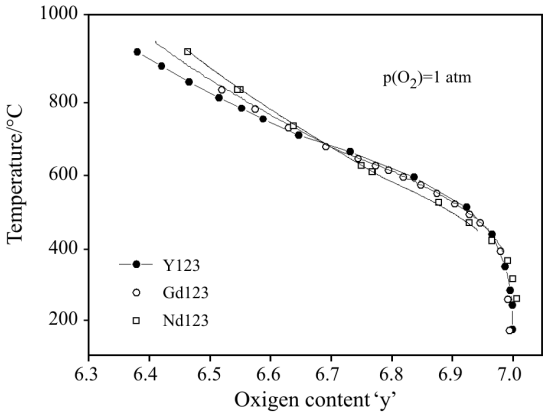

Fig. 6 *T vs. y* curves under pure oxygen for ● – Y123, ○ – Gd123 and □ – Nd123 obtained through equilibrium measurements after a step change in $p(O_2)$. The solid lines correspond to measurements performed during heating at 1°C min^{-1}

served that at high temperatures the R123 compounds with larger R ion radii ($r_{Gd}^{3+} > r_{Nd}^{3+} > r_{Y}^{3+}$) display a smaller oxygen non-stoichiometry. On the other hand, the maximum oxygen content at lower temperature occurs at practically the same value of 'y', that is y=7.00 for Y123, Gd123 and Nd123. From the discontinuity existing in the first derivative of the *T vs. y* curves one can determine the values of $y_{O/T}$ and $T_{O/T}$ under constant $p(O_2)$.

Hence, isobars performed under different $p(O_2)$ values allow the determination of the *O*/*T* transition. Early neutron diffraction measurements of Jorgensen *et al*. [45] have shown that the variation of the cell parameters is continuous across the *O*/*T* transition and hysteresis is not observed even at low *T* indicating the second order nature for this transition. The *O*/*T* transition can also be determined by X-ray powder diffraction at high temperatures (HTXRD) under controlled $p(O_2)$. In Fig. 7a and b are shown our determination of the lattice parameters as a function of *T* under different $p(O_2)$ atmospheres for Gd123 and Nd123, respectively. We observe a good agreement between both experimental procedures. In Fig. 8 are summarized the *O*/*T* transition of selected literature data for Y123 [45–49], Gd123 [18, 19], Nd123 [18] and our data obtained by thermogravimetry and HTXRD for Gd123 and Nd123. In spite of the appreciably scatter of the literature data for Y123, it is clear that the *O*/*T* border line transition is shifted toward lower temperatures as the *R* atom ion size increases. Further information on this study can be found in [32] and the references therein.

Figure 9 shows the equilibrium $p(O_2)$ values as a function of oxygen content for Gd123 determined by isothermal measurements within the temperature range 450≤*T*≤800°C. We have included in this plot

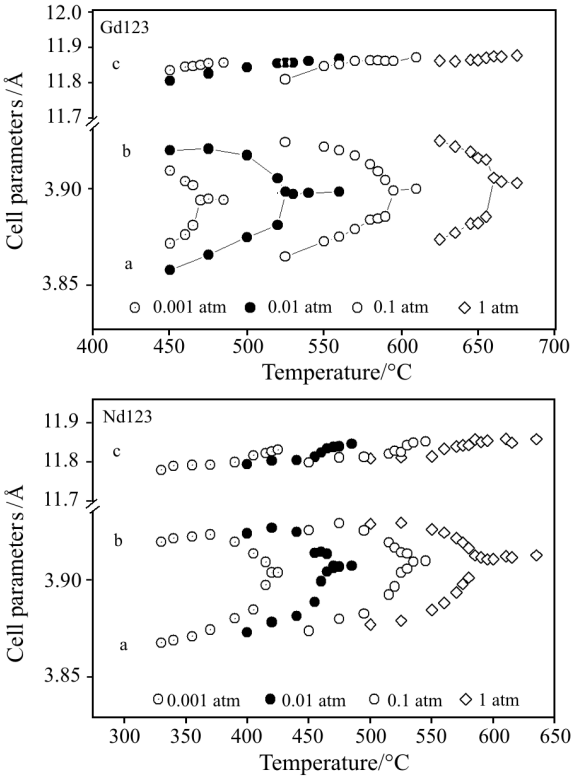

Fig. 7 Lattice parameters *a*, *b* and *c* as a function of *T* obtained under different $p(O_2)$ atmospheres for Gd123 and Nd123, respectively

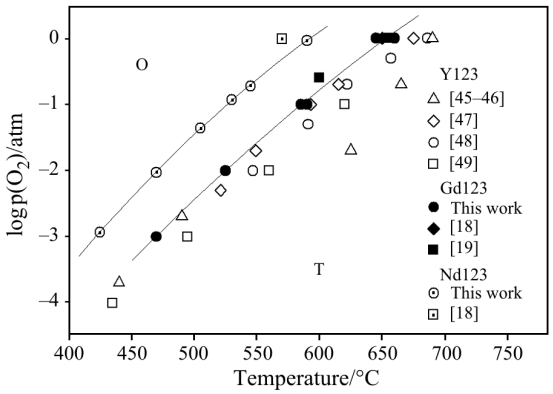

Fig. 8 Log$p(O_2)$ as a function of *T* for the *O*/*T* transition for Gd123 and Nd123 determined in the present work and literature data for Y123, Gd123 and Nd123. The solid lines was drawn as eye guide

the *O*/*T* transition obtained by means of HTXRD. In Fig. 10, the log$p(O_2)$ *vs*. *y* data for Gd123 at 600 and 800°C and Nd123 at 600°C are compared with those of Y123 taken from [50].

Significant differences between the isotherms at 800°C for the three compounds in the tetragonal region can be observed. The oxygen content increases with the ionic radii of the *R* atom at constant $p(O_2)$. These increment clearly indicate that the R123 compounds

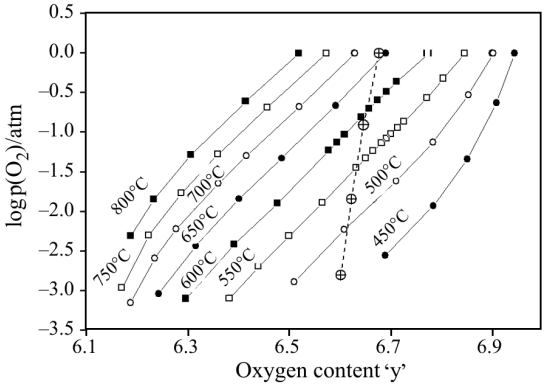

Fig. 9 Log$p(O_2)$ *vs. y* data for Gd123 at different temperatures. The broken line indicates the *O*/*T* transition de-

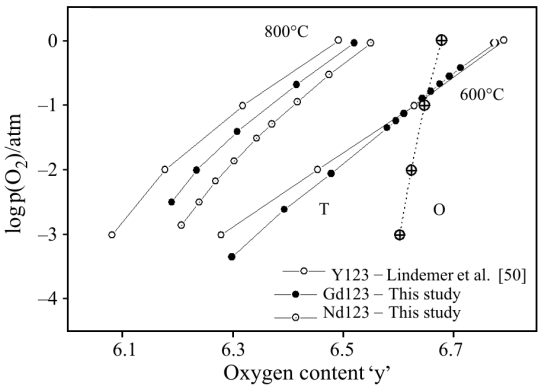

Fig. 10 Log$p(O_2)$ *vs. y* curves at 800°C for Y123, Gd123 and Nd123 and at 600°C for Y123 and Gd123

improve their thermodynamic stability as the ionic radii of the *R* atom increases. Therefore, these data are in agreement with the observed increment of the melting point of the R123 compounds with the ionic radii of *R* [18–20]. In Fig. 11, we confirm this fact by DTA measurements on the three R123 compounds. The endothermic DTA peaks obtained under pure oxygen occurs at 1035, 1073 and 1109°C for the Y123, Gd123 and Nd123 according to the peritectic melting reaction:

$$2RBa_2Cu_3O_y \rightarrow R_2BaCuO_5 + \text{liquid} \quad (8)$$

The same effect on the increment of the melting point has been observed when Ba is partially substituted by Sr in $Y(Ba_{1-x}Sr_x)_2Cu_3O_y$ [51]. Regarding the unit cell parameters, the substitution of Ba by Sr decreases the unit cells parameters for $Y(Ba_{1-x}Sr_x)_2Cu_3O_y$ while the substitution of Y by a larger ion has the opposite effect increasing the lattice parameters.

A plausible explanation for the increment of the cohesive energy for both R123 and Ba substituted 123 compound can be found using the concept of lattice mismatch between Ba–O and Cu(2)–O_2 layer as described by the Goldschmidt tolerance factor *t*:

$$t = (\text{Ba–O})/\sqrt{2}(\text{Cu–O}) \quad (9)$$

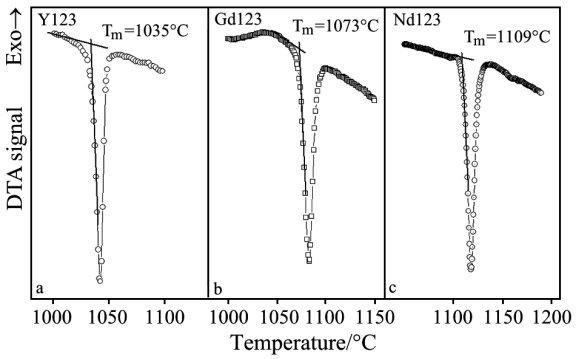

Fig. 11 DTA curves as a function of *T* showing the peritectic reaction for samples of a – Y123, b – Gd123 and c – Nd123

Ba–O and Cu–O are the equilibrium bond lengths. For 123 compounds '*t*' is close to 1 at room temperature and increases as *T* increases due to the larger thermal expansion of the Ba–O bonds relative to that of the Cu–O [52]. Therefore, at high temperature the Ba–O layers should be subjected to compressive stress while the Cu–O to tensile stress.

The substitution of Ba by a smaller ion such as Sr reduces the tolerance factor at high temperature with the consequent increment on the solid phase stability and therefore on the melting point.

Another possibility to release the stress on the Ba–O layer at high temperatures is to allow an expansion of this layer. This could be achieved by the substitution of Y by a larger ion such as Gd permitting the diminution of the compressive stress on the Ba–O layer at high temperatures and therefore the increment of the cohesive energy. Thus, based on the criteria of the lattice mismatch between Ba–O and Cu–O layers, the cohesive energy of the R123 compounds increases as the ionic radii of *R* increases similarly to that occurred for $Y(Ba_{1-x}Sr_x)_2Cu_3O_y$.

$Hg_{1-x}Re_xBa_2CuO_{4+\delta}$ material

Figure 12 shows the unit cell of the Hg(Re)-1201 compound proposed by Kishio *et al.* [53] and Chmaissem *et al.* [54] from Rietveld refinements of neutron powder diffraction data. This figure shows the existence of two types of oxygen crystallographic sites in the Hg–O_δ plane. One of them, the O(3) site, corresponds to that of the oxygen doping for the Re-free samples ($HgBa_2CuO_{4+\delta}$). The other one, the O(4) site, is related to the oxygen atoms bonded to each Re cation. According to this model, each Re atom introduces four extra oxygen atoms in the structure of the 1201 phase.

Figure 13 displays the X-ray diffraction patterns of $Hg_{1-x}Re_xBa_2CuO_{4+\delta}$ samples annealed at 300°C under pure oxygen. These data indicate the existence

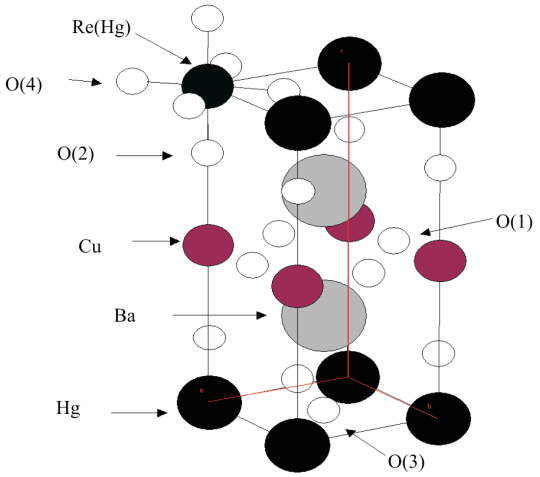

Fig. 12 Unit cell of the (Hg, Re)-1201 compound, which corresponds to the tetragonal system

of single phase materials for x values up to 0.20. We also observed a variation of the lattice as a function of Re content which also suggests the full incorporation of Re cations in the structure of the 1201 material.

The lattice parameters were obtained by Rietveld refinements in the P4/mmm space group. It is interesting to note that the lattice parameters can be accurately determined by this method while the relative intensity of the X-ray reflections are difficult to refine. This may be due to a lack of knowledge of the right occupancy number and the exact position of the heavy atoms in the structure of the (Hg, Re)-1201 phase. It is worth mentioning that some authors have proposed Hg deficiency in the Hg–O_δ planes [55, 56], while others suggested a partial substitution of Hg by Cu or CO_3^{2-} ions [25, 56]. None of these last alternatives allowed us to improve the quality of the refinements, suggesting that the true structural model may include any subtle change in the atomic positions and occupancy numbers.

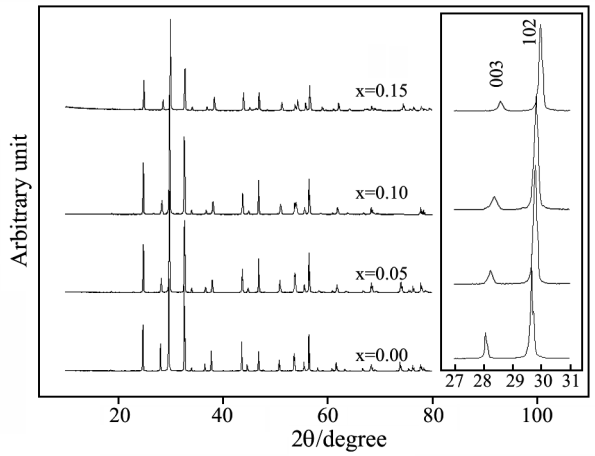

Fig. 13 Powder X-ray diffraction data for $Hg_{1-x}Re_xBa_2CuO_y$ samples

The quality of the samples was also checked by SEM and EDS analysis. Well-developed grains of around 10–20 μm were observed in all samples. Occasionally and after a carefully observation of the sample, the presence of isolated traces of a secondary phase containing Ba and Cu was detected.

In contrary to the general statement that the undoped Re samples undergo a rapid degradation under ambient atmospheres, we found by SEM observations that our Re-free samples remain stable during several months under ambient conditions. The T_{co} and Meissner fraction did not show any change with time either. We believe that the high stability of the Re-free samples may be due to the excess of HgO in the starting HgO–$Ba_2CuO_{3+\delta}$ mix. This excess would avoid the formation of secondary phases composed by Ba and Cu oxides which are responsible of such degradation in samples with Hg deficiency.

Figures 14a–c display the equilibrium $p(O_2)$ measurements as a function of oxygen content 'y' for the x=0.00, x=0.10 and x=0.20 samples. The absolute oxygen content values were computed from data obtained by the NPD refinement for samples annealed under pure oxygen at 300°C. The $p(O_2)$ equilibrium data were verified over 24 h periods within ±10 μg. For the x=0.00 sample, the isotherms below 300°C were reproducible under systematic oxidation or reduction. An exception of this was the low-pressure data points of the 350°C isotherm, which presented a continuous drift of the mass sample indicating a loss of stability for the x=0.00 sample. The oxidation of this sample from these T and $p(O_2)$ values leads to sample mass values lower than those previously obtained. This fact indicates that a decomposition process takes place in the x=0.00 sample at 350°C and low $p(O_2)$ values. This process may involve a Hg content loss in the sample [57].

The temperature of the beginning of the decomposition process increases as the Re content increases. For the x=0.10 sample, this temperature is 400°C while for the x=0.15 one is higher than 500°C, indicating an improvement on chemical stability of the Hg-1201 phase with Re doping.

It can be seen in Fig. 14 that the overall oxygen content values for the Re doped samples are higher than those of the Re-free ones. This is due to the high oxidation state of this element (6+). The difference on the oxygen content values between x=0.00, x=0.10 and x=0.15 samples indicates that each Re cation bonds roughly four extra oxygen atoms to the structure, in agreement with the model proposed by Chmaissen *et al.* [53].

Besides, the $p(O_2)$ measurements show that the oxygen non-stoichiometry range as a function of $p(O_2)$ decreases as the Re content increases. This fact

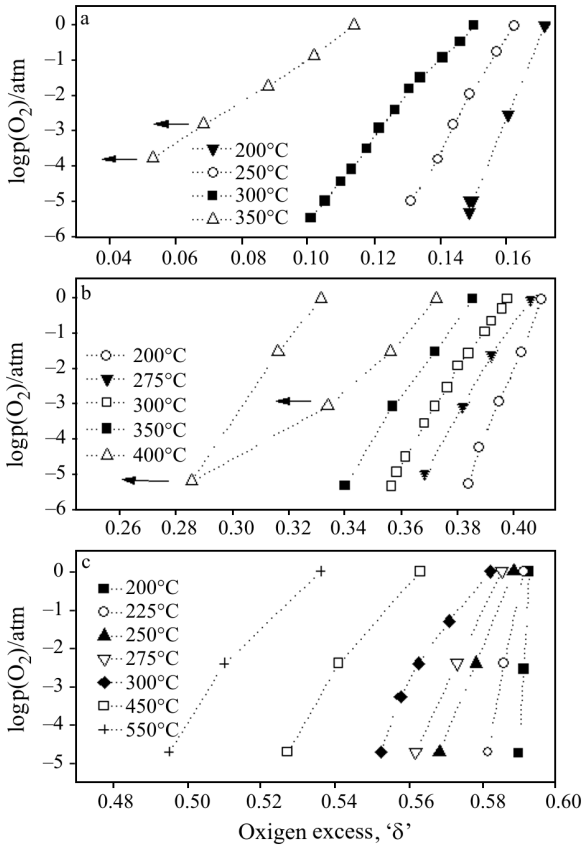

Fig. 14 Log$p(O_2)$ *vs.* oxygen content for $Hg_{1-x}Re_xBa_2CuO_y$ samples. a – x=0, b – x=0.10, c – x=0.15. The arrows indicate non-equilibrium points

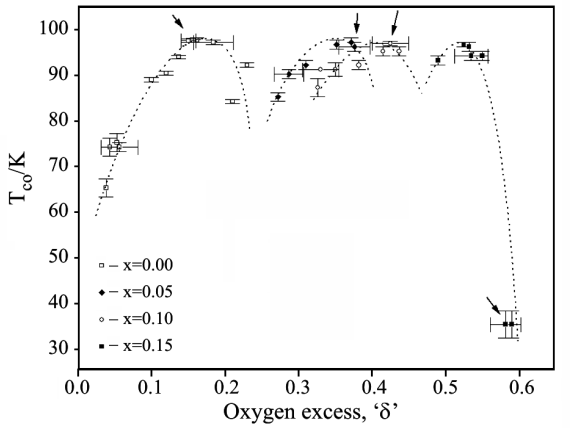

Fig. 15 T_{co} as a function of oxygen excess 'δ' for samples of $Hg_{1-x}Re_xBa_2CuO_{4+\delta}$ prepared with controlled oxygen

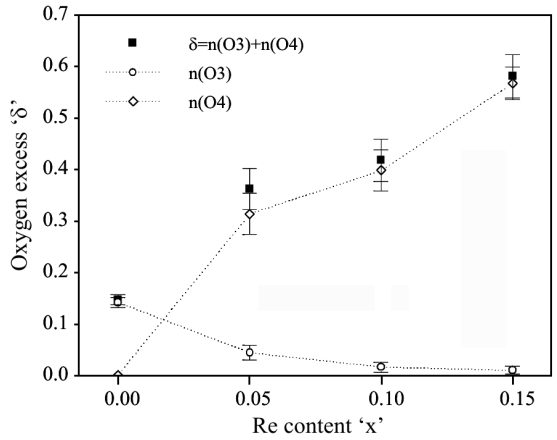

Fig. 16 O(3) and O(4) occupancy numbers [n(O3) and n(O4)] determined by NPD for samples annealed at 300°C under 1 atm of pure oxygen

reveals a stabilization of the oxygen sublattice as a function of the Re content indicating that, in the (Hg, Re)–O_δ plane, the O(4) oxygen atoms are more strongly bounded than the O(3) ones.

The T_{co} is plotted in Fig. 15 as a function of the oxygen content for x=0.00, 0.05, 0.15 and 0.15 samples. The oxygen contents were determined by thermogravimetry taking as a reference those oxygen content values determined by NPD; the later are indicted by arrows in Fig. 15. It can be observed that the Re doping does not produce any significant change on the optimal T_{co}, that is $T_{c\ max}$. $T_{c\ max}$ slightly decreases (from 97.4 to 96 K) with Re content which could be caused by a cation disorder affecting the electronic structure.

In order to discuss the effect of oxygen excess 'δ' on T_c the O(3) and O(4) occupancy numbers [n(O3) and n(O4)] determined by Rietveld refinements of the NDP data for samples annealed at 300°C under 1 atm of pure oxygen are shown in Fig. 16. These data show that for Re-free samples, the oxygen excess (δ) is localized at the O(3) crystallographic site determining the carrier concentration. Besides, nO(3) decreases as Re content increases and is practically zero for x>0.05 samples. Therefore, for the (Hg, Re)-1201 samples, the O(4) oxygen atoms dope holes into the CuO2 planes playing a crucial role on the presence of superconductivity [57].

Conclusions

- High temperature $p(O_2)$ and resistivity measurements are a powerful tool to study the defect structure of complex oxides materials. From this information it is possible to analyze different types of lattice defects. These measurements allow the determination of the stability range of these materials as a function of T, oxygen content and doping content.
- From the information given by the high temperature thermodynamic data, samples with accurate control of oxygen content can be prepared.
- The variations of the physical properties (transport and magnetic) can be accurately correlated with the oxygen content of the samples and therefore with its defect structure.

- HTSC materials are complex oxides where small variations of the oxygen content can produce dramatic effects on their superconducting behavior. The understanding of such materials requires a suitable knowledge of their defect structure. We suggest for the $Nd_{1.85}Ce_{0.15}Cu_{1.01}O_y$ material that a subtle modification of the crystal lattice due to the presence of microstrains could be the cause of the lack of superconductivity in the as-made samples.
- The high temperature thermodynamic measurements are a useful tool to study the stability of HTSC such as the R123 compounds. The thermodynamic stability improves as the ionic radii of the *R* atom increases This effect is discussed in terms of the lattice mismatch between Ba–O and Cu–O_2 layers.
- The role of the Re doping in the Hg-1201 materials is evidenced by the equilibrium $p(O_2)$ measurements. Re doping increases the high temperature stability at high temperatures due to the incorporation of highly bounded oxygen atoms in the (Hg, Re)–O_δ planes. These extra oxygen atoms dope holes into the CuO_2 planes playing a crucial role on the superconductivity of the (Hg, Re)-1201 material.

Acknowledgements

The authors acknowledge Dr. J. Jorgensen, Dr. J. Hodges and Dr. S. Short for the NPD measurements.

We gratefully acknowledge the help of Eng. M. Esquivel in the English revision of this manuscript.

This work was supported by CNEA (Argentine Atomic Energy Commission), CONICET (Argentine National Research Council), CEB (Bariloche Electricity Company) and CEE (Commission of the European Communities) through DGXII Contract CII *CT92-0087.

References

1 Y. Tokura, H. Takagi and S. Uchida, Nature, 337 (1989) 345.
2 H. Takagi, S. Uchida and Y. Tokura, Phys. Rev. Lett., 62 (1989) 1197.
3 J. M. Tarascon, E. Wang, L. H. Greene, R. Ramesh, B. G. Bagley, G. W. Hull, P. F. Micelli, Z. Z. Wang, D. Brawner and N. P. Ong, Physica C, 162–164 (1989) 285.
4 E. Moran, A. I. Nazzal, T. C. Huang and J. B. Torrance, Physica C, 160 (1989) 30.
5 P. W. Klamut, J. Alloy Comp., 194 (1993) L5.
6 Y. T. Zhu and A. Manthiram, Physica C, 224 (1994) 256.
7 I. Magelschots, N. H. Andersen, B. Lebech, A. Wisniewski and C. S. Jacobsen, Physica C, 203 (1992) 369.
8 P. G. Radaelli, J. D. Jorgensen, A. J. Schultz, J. L. Peng and R. L. Greene, Phys. Rev. B, 49 (1994) 15322.
9 T. Kawashima and E. Takayama-Muromachi, Physica C, 219 (1994) 389.
10 Y. Idemoto, K. Fueki and T. Shimbo, Physica C, 166 (1990) 513.
11 K. Suzuki, K. Kishio, T. Hasegawa and K. Kitazawa, Physica C, 166 (1990) 357.
12 J. S. Kim and D. R. Gaskell, Physica C, 209 (1993) 381.
13 F. Prado, A. Caneiro, J. Briatico and A. Serquis, Sol. State Comm., 94 (1995) 75.
14 K. Kishio, T. Hasegawa, K. Suzuki, K. Kitazawa and K. Fueki, Mat. Res. Soc. Symp. Proc., 56 (1989) 91.
15 M. Tatenbaum, B. Tani, B. Czech and M. Blander, Physica C, 158 (1989) 377.
16 M. Tatenbaum, P. Tumidajski, D. L. Brown and M. Blander, Physica C, 198 (1992) 109.
17 H. Ishizuka, Y. Idemoto and K. Fueki, Physica C, 195 (1992) 145.
18 Y. Kubo, Y. Nakabayashi, J. Tabuchi, T. Yoshitake, T. Manako, A. Ochi, K. Utsumi, H. Igarashi and M. Yonezawa, Mat. Res. Soc. Symp. Proc., 99 (1988) 89.
19 M. Kogachi, S. Nakanishi, K. Nakahigashi, H. Saakura, S. Minamigawa, N. Fukuoka and A. Yanase, Jpn. J. Appl. Phys., 28 (1989) L609.
20 M. Kogachi, K. Nakahigashi, S. Minamigawa and S. Nakanishi, Jpn. J. Appl. Phys., 29 (1990) L911.
21 S. N. Putilin, E. V. Antipov, O. Chmaissem and M. Marezio, Nature, 363 (1993) 226.
22 J. F. Marucco, V. Viallet, A. Bertinotti, D. Colson and A. Forget, Physica C, 275 (1997) 12.
23 A. Fukuoka, A. Tokiwa-Yamamoto, M. Itoh, R. Usami, S. Adachi, H. Yamauchi and K. Tanabe, Physica C, 265 (1996) 13.
24 Q. Xiong, Y. Xve, Y. Kao, F. Chen, Y. Sun, J. Gibson, C. W. Chu, L. M. Liu and A. Jacobson, Phys. Rev. B, 50 (1994) 10346.
25 S. M. Loureiro, E. T. Alexandre, E. V. Antipov, J. Capponi, S. Brion, V. Souletie, J. L. Tholence and M. Marezio, Physica C, 243 (1995) 1.
26 A. Maignan, D. Pelloquin, S. Malo, C. Michel, M. Hervieu and B. Raveau, Physica C 243 (1995) 233.
27 K. Przybylski, T. Brylewski, A. Morawski and T. Lada, J. Therm. Anal. Cal., 65 (2001) 391.
28 S. Mathur, H. Shen, N. Lecerf, M. H. Jilavi, V. Cauniene, J. Jorgensen and A. Kareiva, J. Sol-Gel Sci. Technol., 24 (2002) 57.
29 G. W. Chadznski, V. V. Kutarov and P. Staszczuk, J. Therm. Anal. Cal., 76 (2004) 633.
30 M. Karppinen, H. Yamauchi, Y. Morita, M. Kitabatake, T. Motohashi, R. S. Liu, J. M. Lee and J. M. Chen, J. Solid State Chem., 177 (2004) 1037.
31 A. Serquis, A. Caneiro and F. Prado, Physica C, 331 (1999) 271.
32 F. Prado, A. Caneiro and A. Serquis, Physica C, 295 (1998) 235.
33 M. Ochsenkühn-Petropulu, P. Tarantilis, R. Argyropulu and G. Parissakis, J. Thermal Anal., 52 (1998) 903.
34 A. Caneiro, P. Bavdaz, J. Fouletier and J. P. Abriata, Rev. Sci. Instrum., 53 (1982) 1072.
35 F. Prado, J. Briático, A. Caneiro, M. Tovar and M. T. Causa, Solid State Commun., 90 (1994) 695.
36 A. Serquis, F. Prado and A. Caneiro, Physica C, 273 (1996) 163.
37 V. A. Alyoshin, D. A. Mikhailova and E. V. Antipov, Physica C, 255 (1995) 173.
38 R. A. Young, A. Sakthivel, T. S. Moss and C. O. Paiva-Santos, J. Appl. Crystallogr., 28 (1995) 366.

39 F. A. Kröger, 'The Chemistry of Imperfect Crystals', North Holland Publishing Co., Amsterdam 1964.
40 F. Prado, A. Caneiro and A. Serquis, J. Thermal Anal., 48 (1997) 1027.
41 A. Fainstein, A. Serquis, R. G. Pregliasco, F. Prado and A. Caneiro, Phys. Rev. B., 63 (2001) 184503.
42 D. R. Knittel, S. P. Pack, S. H. Lin and L. Eyring, J. Chem. Phys., 67 (1977) 134.
43 H. Inaba, S. P. Pack, S. H. Lin and L. Eyring, J. Solid State Chem., 33 (1980) 295.
44 S. Asbrink and L. Norby, Acta Cryst. B, 26 (1970) 8.
45 J. D. Jorgensen, M. A. Beno, D. G. Hills, L. Soderholme, K. J. Volin, R. L. Hitterman, J. D. Grace, I. K. Schuller, C. E. Segre, K. Zhang and M. S. Klefisch, Phys. Rev. B, 36 (1987) 3608.
46 J. D. Jorgensen, B. W. Veal, A. P. Paulikas, L. J. Nowicki, G. W. Crabtree, H. Claus and W. K. Kwok, Phys. Rev. B, 41 (1990) 1863.
47 E. D. Specht, C. J. Sparks, A. G. Dhere, J. Brynestad, O. B. Cavin, D. M. Kroeger and H. A. Oye, Phys. Rev. B, 37 (1988) 7426.
48 Y. Kubo, Y. Nakabayashi, J. Tabuchi, T. Yoshitake, A. Ochi, K. Utsumi, H. Igarashi and M. Yonezawa, Jpn. J. Appl. Phys., 26 (1987) L1888.
49 J. Mizusaki, H. Tagawa, K. Hayakawa and K. Hirano, J. Am. Ceram. Soc., 78 (1995) 1781.
50 T. N. Lindemer, J. F. Hunley, J. E. Gates, A. L. Sutton Jr., J. Brynestad, C. R. Hubbard and P. K. Gallagher, J. Am. Ceram. Soc., 72 (1989) 1775.
51 E. Oliber, C. González Oliver, F. Prado, A. Serquis, A. Caneiro and D. Esparza, Physica C, 235–240 (1994) 469.
52 J. B. Goodenough and A. Manthiram, J. Solid State Chem., 88 (1990) 115.
53 O. Chmaissem, P. Guptasarma, U. Welp, D. G. Hinks and J. D. Jorgensen, Physica C, 292 (1997) 305.
54 K. Kishio, J. Shimoyama, A. Yoshikawa, K. Kitazawa, O. Chmaissem and J. D. Jorgensen, J. Low Temp. Phys., 105 (1996) 1359.
55 A. Asab. A. Armstrong, I. Gameson and P. Edwards, Physica C, 255 (1995) 180.
56 J. L. Wagner, P. G. Radaelli, D. G. Hinks, J. D. Jorgensen, J. F. Mitchell, B. Dabrowski, G. Knapp and M. Beno, Physica C, 210 (1993) 447.
57 A. Serquis, A. Caneiro, A. Basset, S. Short, J. P. Hodges and J. D. Jorgensen, Phys. Rev. B, 63 (2000) 014508.

Received: July 21, 2005
Accepted: August 16, 2005

DOI: 10.1007/s10973-005-7226-2